FISEVIER

Contents lists available at ScienceDirect

# **Progress in Surface Science**

journal homepage: www.elsevier.com/locate/progsurf



# Review article

# STM studies of photochemistry and plasmon chemistry on metal surfaces



Emiko Kazuma<sup>a</sup>, Jaehoon Jung<sup>b</sup>, Hiromu Ueba<sup>c</sup>, Michael Trenary<sup>d</sup>, Yousoo Kim<sup>a,\*</sup>

- <sup>a</sup> Surface and Interface Science Laboratory, RIKEN, Wako, Saitama 351-0198, Japan
- <sup>b</sup> Department of Chemistry, University of Ulsan, 93 Daehak-ro, Nam-gu, Ulsan 44610, Republic of Korea
- <sup>c</sup> Graduate School of Science and Engineering, University of Toyama, Toyama 930-8555, Japan
- <sup>d</sup> Department of Chemistry, University of Illinois at Chicago, 845 W Taylor Street, Chicago, IL 60607, United States

## ARTICLE INFO

Keywords: Scanning tunneling microscope (STM) Photochemistry Plasmon chemistry Photochemical reaction Plasmon-induced chemical reaction Single molecule Surface reaction Reaction mechanism Reaction pathway Direct intramolecular excitation Density of states (DOS) Chemisorption Metal surfaces Dimethyl disulfide (CH<sub>3</sub>S)<sub>2</sub> Transient negative ion (TNI) Density functional theory (DFT) Inelastic electron tunneling spectroscopy (IETS) STM action spectroscopy (STM-AS)

#### ABSTRACT

We review our recent studies of photochemistry and plasmon chemistry of dimethyl disulfide,  $(CH_3S)_2$ , molecules adsorbed on metal surfaces using a scanning tunneling microscope (STM). The STM has been used not only for the observation of surface structures at atomic spatial resolution but also for local spectroscopies. The STM combined with optical excitation by light can be employed to investigate chemical reactions of single molecules induced by photons and localized surface plasmons. This technique allows us to gain insights into reaction mechanisms at a single molecule level. The experimental procedures to examine the chemical reactions using the STM are briefly described. The mechanism for the photodissociation reaction of  $(CH_3S)_2$  molecules adsorbed on metal surfaces is discussed based on both the experimental results obtained with the STM and the electronic structures calculated by density functional theory. The dissociation reaction of the  $(CH_3S)_2$  molecule induced by the optically excited plasmon in the STM junction between a Ag tip and metal substrate is also described. The reaction mechanism and pathway of this plasmon-induced chemical reaction are discussed by comparison with those proposed in plasmon chemistry.

# 1. Introduction

Local density of states (LDOS)

The effective conversion from clean and renewable solar energy to chemical energy by inducing chemical reactions is increasingly required for modern industry. In the 1990s, photodissociation and photodesorption of the molecules adsorbed on metal surfaces was enthusiastically studied [1-23]. Novel reaction pathways different from those in the gas and liquid phases can be provided by the interaction between the molecules and metal surfaces, which defines the interfacial electronic structures. Most photochemical reactions of small molecules  $(O_2, CH_4, Cl_2CO, etc.)$  on single-crystalline metal surfaces have been achieved with UV light.

In photochemistry on metal surfaces (far-field chemistry), three principal mechanisms have been proposed (Fig. 1(a)) on the basis of experiments with spectroscopies such as temperature-programmed desorption-mass spectroscopy, high-resolution electron energy-

https://doi.org/10.1016/j.progsurf.2018.08.003

<sup>\*</sup> Corresponding author.

E-mail address: ykim@riken.jp (Y. Kim).

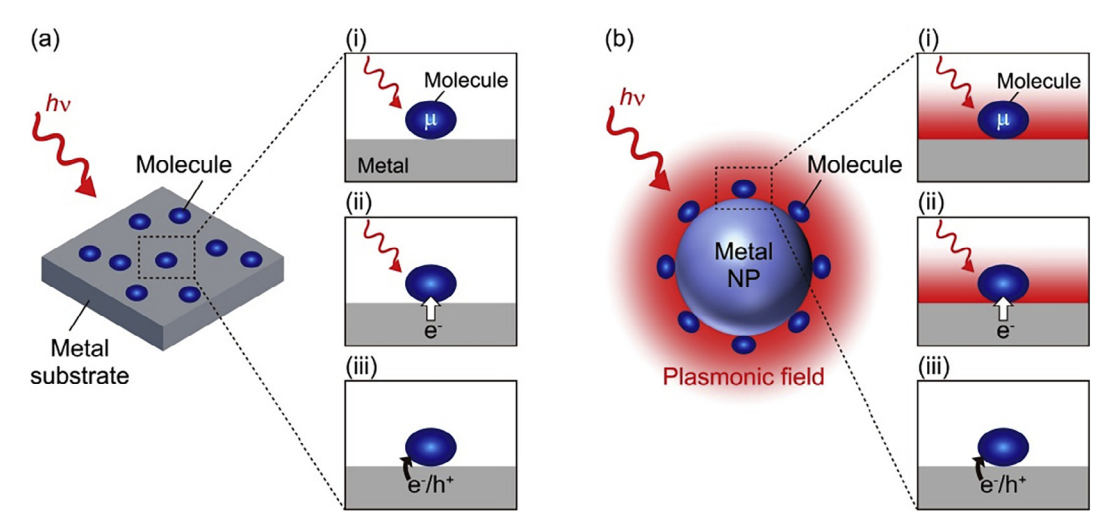


Fig. 1. Excitation mechanisms in (a) photochemistry on a metal substrate and (b) plasmon chemistry on a metal nanoparticle (NP). (i) Direct intramolecular excitation mechanism, (ii) charge-transfer mechanism, and (iii) indirect hot-electron transfer mechanism.

loss spectroscopy [3-18] and two-photon photoemission (2PPE) [19-23], as described in detail in Section 3.

Excitation mechanisms in photochemistry on metal surfaces (far-field chemistry) (Fig. 1(a)) are as follows:

- (i) Direct intramolecular excitation (coupling between a transition dipole (µ) with the electric field of the light)
- (ii) Charge transfer (direct excitation) from bulk or surface states to unoccupied molecular orbitals
- (iii) Indirect hot-electron transfer to the unoccupied molecular orbitals (hot electrons are generated by light absorption by the metals)

In the past 10 years, on the other hand, plasmon-induced chemical reactions on metal nanostructures such as Au and Ag nanoparticles have been attracting attention because the plasmon can promote more highly efficient conversion from solar energy to chemical energy than in the case of photochemical reactions [24–57]. The plasmon resonantly excited by light generates a strong electric field localized near the metal surface and serves as a highly efficient excitation source. Formation of an azo bond was found and observed by the change in the spectra of surface-enhanced Raman scattering (SERS) [26–31] and tip-enhanced Raman scattering (TERS) [32–35]. Dissociation of  $O_2$  [44,46] and  $O_2$  H2 [47,52] molecules was achieved also by the plasmon of metal nanoparticles, which was proven by the detection of the produced molecules with gas chromatography.

Immediately after the excitation of the plasmon, hot electrons and holes are created in metal nanostructures through nonradiative decay of the plasmon, and finally the plasmon energy is thermally dissipated. During the decay process, four proposed mechanisms are available in the plasmon-induced chemical reactions. However, it is still unclear which factor determines the principal mechanism.

Excitation mechanisms in plasmon chemistry on metal surfaces (near-field chemistry) (Fig. 1(b)) are as follows:

- (i) Direct intramolecular excitation (coupling between transition dipole (μ) with the electric field of the plasmon)
- (ii) Charge transfer (direct excitation) from near the Fermi level to the unoccupied molecular orbitals
- (iii) Indirect hot-electron transfer to the unoccupied molecular orbitals (hot electrons are generated by light absorption of metal nanostructures due to the plasmon)
  - (iv) Local heating effect

The different excitation mechanisms result in different reaction pathways because the initial excited states are different [1]. In the case of (i) direct intramolecular excitation, the excited state is neutral because the separated holes and electrons exist in the molecule. In contrast, in both cases of (ii) charge transfer and (iii) indirect hot-electron transfer, the excited state involves a transient negative ion (TNI). It is difficult to discriminate (ii) and (iii) by experiments. Charge transfer is resonant excitation from the metal states to the adsorbate state (one-step process), whereas indirect hot-electron transfer includes the light absorption of metals, the creation of hot carriers, and electron transfer to the unoccupied molecular orbitals (three-step process) [58]. Therefore, in photochemistry on metal surfaces, only time-resolved spectroscopy would distinguish them clearly [59,60]. In plasmon chemistry, most cases have been explained by the indirect hot-electron transfer mechanism without direct evidence. However, the mechanism of the plasmon-induced chemical reaction is still a subject worth further investigation.

The main problem of chemical reactions on metal surfaces induced by light is that the reactions are suppressed due to the short lifetimes of the excited molecular states caused by the hybridization between molecular orbitals and the metal surfaces. To elucidate the underlying mechanisms of both photochemistry and plasmon chemistry on the metal surfaces, a fundamental understanding of the relationship between the reaction pathways and the interfacial electronic structures is crucial.

A scanning tunneling microscope (STM) can provide mechanistic insight based on the real-space investigation of photochemical reactions on metal surfaces. The atomically well-defined surfaces of metal single crystals are necessary to obtain molecular-scale mechanistic insights, which enable the combination of experiments with the STM and density functional theory (DFT) calculations to

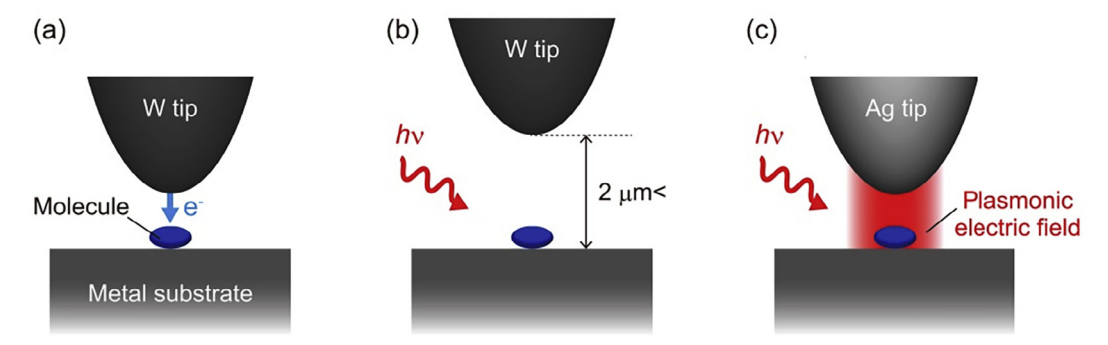


Fig. 2. Schematic illustrations of experiments using an STM for (a) IET-induced reactions, (b) photochemical reactions, and (c) plasmon-induced chemical reactions.

investigate surface photochemical reactions and the accompanying changes in the electronic structure. Furthermore, STM can be applied to investigate the plasmon-induced chemical reactions of a single molecule. The findings obtained using the STM provide deep insights into reaction mechanisms at the single-molecule level that cannot be accessed by macroscopic analysis methods.

In this review, we summarize our recent STM studies clarifying the reaction mechanisms responsible for both photodissociation and the plasmon-induced dissociation of dimethyl disulfide,  $(CH_3S)_2$ , molecules adsorbed on Ag(111) and Cu(111) surfaces [61,62]. We discuss the reaction mechanisms proposed in the fields of surface photochemistry and plasmon chemistry in terms of molecular excitation on metal surfaces. Section 2 describes the experimental procedures and techniques of STM investigations of chemical reactions. Section 3 explains the reaction mechanism of the photodissociation reaction of the  $(CH_3S)_2$  molecules on the metal surfaces, which was revealed by STM investigations and DFT calculations. Section 4 summarizes the excitation mechanism and reaction pathway of the plasmon-induced dissociation reaction of the  $(CH_3S)_2$  molecules using the STM.

# 2. Experimental methods for STM investigations of chemical reactions

The STM is a powerful tool not only for observing surface structures at atomic spatial resolution but also for performing local spectroscopies such as scanning tunneling spectroscopy (STS) and inelastic electron tunneling spectroscopy (IETS). The IET process can induce vibrationally mediated motion or reaction of a single molecule in a tunnel junction of an STM (Fig. 2(a)). STM action spectroscopy (STM-AS) provides the elementary processes of IET-induced vibrational excitation resulting in molecular motion or reaction [63].

The combination of optical excitation and detection with the STM has been applied to local spectroscopies such as STM-induced luminescence [64–66] and STM tip-enhanced Raman scattering [67]. In particular, the STM combined with optical excitation has been also applied to investigation of photon-induced molecular motions and dynamics [68–71] or chemical reactions such as photoisomerization [72,73] (Fig. 2(b)). It can be extended to chemical reactions induced by the plasmon optically excited in the STM junction between a plasmonic tip and metal substrate (Fig. 2(c)) [62]. Here, we describe the experimental methods using the STM for IET-induced, photochemical, and plasmon-induced chemical reactions of (CH<sub>3</sub>S)<sub>2</sub> molecules.

# 2.1. Experimental setup and sample preparation

All experiments were performed with a low-temperature STM (Omicron GmbH) maintained at 5 K under an ultra-high vacuum of less than  $4.0 \times 10^{-11}$  Torr. The p-polarized light was introduced into the STM chamber through a viewport (transmittance  $\geq$  95% at 400–1000 nm) with an incident angle of 25° to the sample surface. The light sources were coupled to an optical fiber. The fiber was connected to an optical cage system (THORLABS) including the optical filters, an iris, and lenses, which was attached to the STM chamber. The light was collected by lenses attached outside of the chamber and focused onto the sample surface with a spot diameter of  $\phi \sim 1.2$  mm. The visible and near infrared light sources were CW lasers (wavelength  $\lambda = 405$ , 450, 520, 532, 635, 650, 670, 780, 850, and 980 nm, Collimated Laser Diode Module, THORLABS) and a Xe lamp with a small emission size ( $\sim$  0.1 mm) directly coupled to the optical fiber (Laser-Driven Light Source, TOKYO INSTRUMENTS, INC) equipped with bandpass filters (THORLABS). The light intensity was tuned with ND filters (THORLABS) and was evaluated in an equivalent sample position with all optical components in the path by using an optical power meter (THORLABS) and a dual scanning slit beam profiler (THORLABS). W tips were used for IET-induced reaction and photochemical reaction (Fig. 2(a, b)) because W has mechanical strength, a relatively flat density of state (DOS) near the Fermi level ( $E_F$ ), and does not contribute to the plasmonic field enhancement. Sharp Ag tips prepared by electrochemical etching were used for the plasmon-induced chemical reactions (Fig. 2(c)).

Ag(111) and Cu(111) single-crystalline substrates were cleaned using repeated cycles of Ar<sup>+</sup>-ion sputtering and annealing, and the (CH<sub>3</sub>S)<sub>2</sub> molecules were deposited by evaporation from a glass ampoule at room temperature. The substrates were maintained at  $< 50 \,\mathrm{K}$  during deposition. The scanning conditions for obtaining STM images were  $V_{\rm s}$  (sample bias voltage) = 20 mV and  $I_{\rm t}$  (tunneling current) = 0.2 nA.

## 2.2. STM investigation of IET-induced, photochemical, and plasmon-induced chemical reactions

IET-induced molecular reaction was achieved by injecting tunneling electrons from the STM tip with the feedback loop turned off, after positioning the tip over the target molecule (Fig. 2(a)). The reaction is manifested as a sudden change in the recorded current traces at a constant bias voltage due to a change in the distance between the tip and the sample (d) (( $I_t \propto V_s$  exp(- $Ad\sqrt{\Phi}$ ) (A: coefficient,  $\Phi$ : barrier height)). The time required for the reaction of a single molecule (t) is read from the current trace and the reaction yield (t) is calculated by t = t/t<sub>e</sub> = t/t<sub>e</sub>. the total number of injected tunneling electrons, t elementary charge). The STM action spectrum is obtained by measuring the applied bias-voltage dependence of t. The details for the experimental procedure of STM-AS are described in [63].

The STM combined with optical excitation by light is applicable to analyze photochemical reactions on surfaces. The sample in the STM chamber was irradiated with light, and during irradiation, the STM tip was retracted more than  $2 \mu m$  from the sample surface to avoid tip-induced effects (Fig. 2(b)). The STM images were measured before and after light irradiation and quantitative information of the photochemical reaction of (CH<sub>3</sub>S)<sub>2</sub> was obtained by analyzing the reaction ratio ( $N/N_0$ ), which is defined as the number of molecules (N) after light irradiation divided by the total number of preadsorbed molecules ( $N_0$ ).

The STM combined with optical excitation can be applied to investigation of the plasmon-induced chemical reaction at a single molecule level. To excite the plasmon optically, the Ag tip was positioned over the bare metal surface or target molecule during light irradiation. Reaction time was obtained by measuring the current trace when the STM tip was first positioned over the target molecule at a fixed tunneling-gap resistance, and then turning off the feedback loop to maintain the tip height during light irradiation (Fig. 2(c)). The tunneling current sensitively detects a change in the gap distance due to the reaction previously described. The time required for the single reaction event induced by the plasmon ( $t_p$ ) is directly read out from the current trace.

## 2.3. DFT calculations

Geometric and electronic structure of an individual  $(CH_3S)_2$  molecule adsorbed on Cu(111) and Ag(111) surfaces were investigated using periodic DFT calculations using Grimme's DFT-D3BJ [74,75] functional and projector augmented wave (PAW) pseudopotentials (the cut-off energy = 400 eV) [76] implemented in the Vienna Ab-initio Simulation Package (VASP) code [77,78]. To minimize the intermolecular interaction among neighboring adsorbates on the surfaces, we employed  $(6 \times 6)$  surface supercells for which a  $4 \times 4 \times 1$   $\Gamma$ -centered grid was used for the k-point sampling of the Brillouin zone. The slab model is composed of a vacuum region of  $\sim 18$  Å and six metal layers, in which the two bottom layers were fixed in their bulk positions during ionic relaxations. The dipole correction was applied to avoid interactions between periodically replicated slab images. The electronic self-consistent iterations and ionic relaxations were carried out with the convergence criteria of  $10^{-7}$  eV and 0.02 eV/Å, respectively.

# 3. Photochemistry of dimethyl disulfide on metal surfaces

In this section, we describe the excitation mechanism of photochemical reactions of  $(CH_3S)_2$  molecules adsorbed on metal surfaces by comparing the previously reported mechanisms of photochemical reactions on the same metal surfaces. The wavelength dependence of the reaction yield was examined to reveal the excitation mechanism. In addition, the DFT calculations provided knowledge of the mechanism to understand the experimental results. For comprehensive understandings of surface photochemistry, we refer the readers to the excellent review by Lindstrom and Zhu [1].

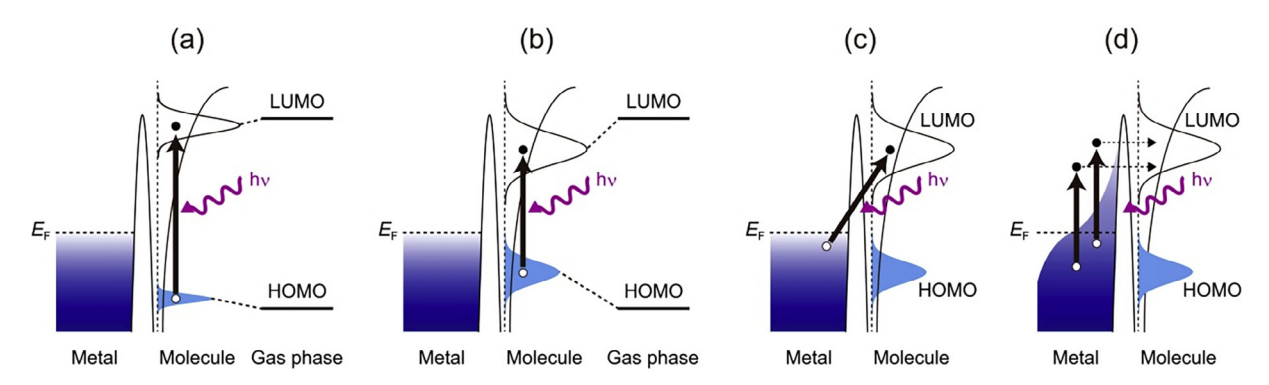


Fig. 3. Excitation mechanisms proposed for photochemical reactions on metal surfaces. (a) Direct intramolecular excitation of physisorbed molecules on a metal surface that has a HOMO–LUMO gap only slightly shifted from its gas-phase value. (b) Direct intramolecular excitation of chemisorbed molecules, in which the electronic states of the molecules are strongly hybridized with the metal states. (c) Charge transfer either from bulk states or from surface states of the metal to the unoccupied molecular orbitals. (d) Indirect hot-electron transfer mechanism. Hot carriers generated by photoabsorption in the bulk metal are transferred to the unoccupied molecular orbitals. Black and white dots indicate electrons and holes, respectively.

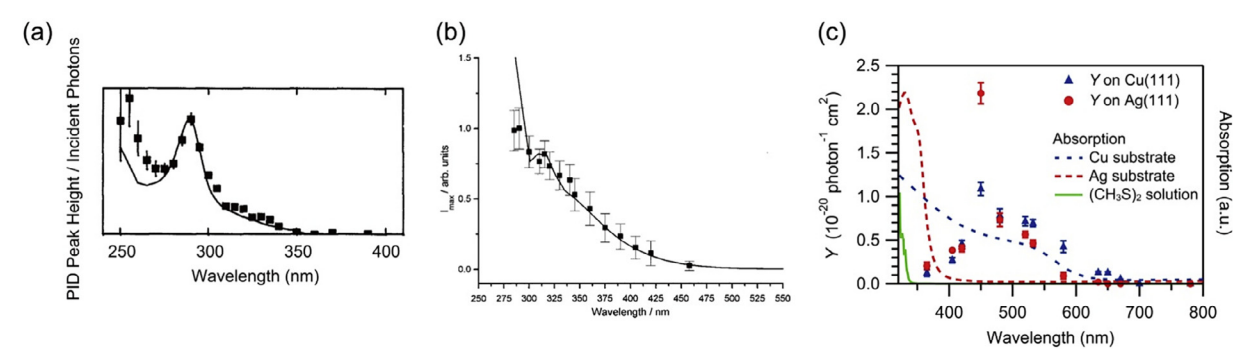


Fig. 4. (a) Wavelength dependence of the photodissociation yield obtained for 1 L Mo(CO)<sub>6</sub> on the Cu(111) surface. The solid line is the absorption spectrum of Mo(CO)<sub>6</sub> measured in cyclohexane solution. Reproduced with permission from [7]. Copyright 1991 AIP Publishing. (b) Wavelength dependence of the dissociative desorption yield of CO from OCS on Ag(111). The solid line is the simulated total yield for dissociative desorption induced by hot-electron attachment. Reproduced with permission from [17]. Copyright 1999 American Chemical Society. (c) Wavelength dependence of photodissociation yield (*Y*) of the (CH<sub>3</sub>S)<sub>2</sub> molecules adsorbed on Cu(111) and Ag(111). The blue and red dotted lines are the simulated absorption spectra of bulk Cu and Ag, respectively. The green line is the absorption spectrum of a (CH<sub>3</sub>S)<sub>2</sub> solution. Reproduced with permission from [61]. Copyright 2017 American Chemical Society. (For interpretation of the references to colour in this figure legend, the reader is referred to the web version of this article.)

## 3.1. Excitation mechanisms and reaction profiles of photochemical reactions on metal surfaces

Fig. 3 shows the excitation mechanisms at molecule–metal interfaces proposed for photochemical reactions on metal surfaces. Photochemical reactions via the direct intramolecular excitation of the frontier electronic states have been reported for molecules physisorbed (Fig. 3(a)) and chemisorbed (Fig. 3(b)) on the metal surfaces. Photodissociation of  $Mo(CO)_6$  molecules on Cu(111) and Cu(111) and Cu(111) is the sole example of the direct intramolecular excitation mechanism for the physisorbed system Cu(111) and Cu(111) dependence of the photodissociation yield for the physisorbed molecules is almost identical to the intrinsic molecular absorption (Fig. 4(a)), which indicates that the electronic levels of the physisorbed molecules are weakly perturbed and the direct excitation across the HOMO–LUMO gap of the adsorbed molecule is induced. Chemisorbed molecules, on the other hand, have molecular orbitals hybridized with the metal states, which results in a narrower energy gap than that in the gas phase. The strong hybridization causes short lifetimes of the molecular excited states, and there are only few examples of photochemical reactions of chemisorbed systems induced by the direct intramolecular excitation. The reaction yield for the chemisorbed system reflects the DOSs of both HOMO and LUMO hybridized with the metal states, and the wavelength dependence of the reaction yield is totally different from the intrinsic molecular absorption. A few chemisorbed systems, such as Cu(10) and Cu(10) on Cu(111) have been analyzed using temperature-programmed desorption after irradiation with UV pulse lasers.

In the charge-transfer mechanism (Fig. 3(c)), electronic coupling between the metal states and the molecular resonance states is necessary. In the case of most single molecules, the coupling term (matrix element) becomes vanishingly small because the anionic molecular resonance state is localized to an individual molecule [79]. Therefore, the charge transfer from the metal states to the molecular states hardly occurs in photochemical reactions of single molecules on metal surfaces, although it was reported for molecular thin films [80,81] and alkali atoms [21,82,83] on metal surfaces.

In contrast, the indirect hot-electron transfer mechanism (Fig. 3(d)) has long been believed to be the primary mechanism for photochemical reactions for numerous adsorbates on metal surfaces. The reaction probability is determined by the density of hot electrons generated through light absorption by the metal. Thus, the wavelength dependence of the reaction yield depends on the energy distribution of the hot electrons, which is determined by the photoabsorption of the metal (Fig. 4(b)) [17].

The real-space investigation using the STM revealed that photodissociation of the S–S bond in  $(CH_3S)_2$  molecules adsorbed on Ag (111) and Cu(111) surfaces was induced by visible-light irradiation (Fig. 5(a)) [61]. The STM images of an individual  $(CH_3S)_2$  molecule adsorbed on the metal surfaces appear as an elliptic protrusion. After light irradiation without the influence of the STM tip (Fig. 2(b)), some of the ellipsoids had broken into two identical ball-shaped protrusions, implying the formation of two  $CH_3S$  molecules due to the dissociation of the S–S bond (Fig. 5(b)). Any other molecular motion such as rotation, translation and desorption, was not observed. Only the molecular photodissociation occurs randomly within the light spot (Fig. 5(c)). This result clearly shows that the reaction is not initiated from the TNI states followed by the vibrational excitation of the molecule, as we will explain in Section 4.

Fig. 4(c) shows the wavelength dependence of the photodissociation yield of  $(CH_3S)_2$  molecules on the metal surfaces. The spectra have a peak at  $\sim$  450 nm ( $\sim$  2.76 eV) on both the Ag and Cu surfaces. The threshold wavelength on the Ag and Cu surfaces is  $\sim$  635 nm ( $\sim$  1.95 eV) and  $\sim$  670 nm ( $\sim$  1.85 eV), respectively. The spectral shape does not match those of intrinsic molecular absorption and metal absorption (Fig. 4(c)), which suggests that the molecules were chemisorbed and the direct intramolecular excitation between hybridized frontier molecular orbitals was induced.

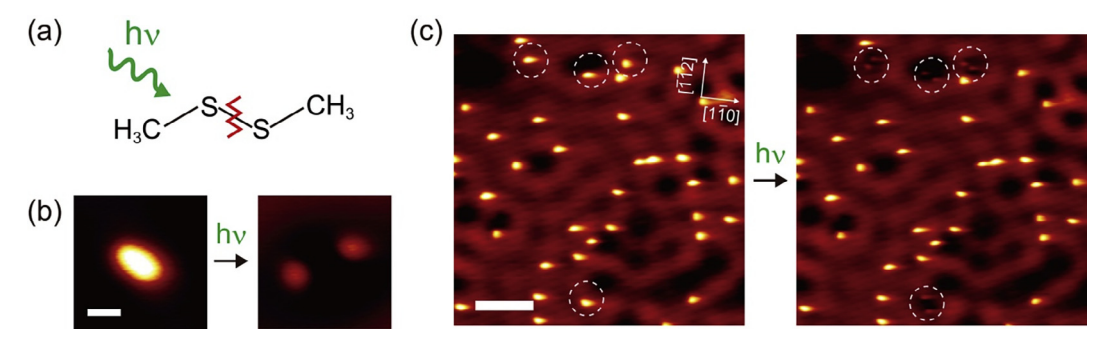


Fig. 5. (a) Structure of a  $(CH_3S)_2$  molecule, indicating the dissociation of the S–S bond by photons. (b, c) Topographic STM images of  $(CH_3S)_2$  molecules adsorbed on Ag(111) before and after irradiation with 532 nm light  $(5.86 \times 10^{16} \, \text{photons cm}^{-2} \, \text{s}^{-1}, \, 10 \, \text{min})$ . The tip was retracted  $\sim 2 \, \mu \text{m}$  from the surface during light irradiation. Dashed circles indicate dissociated molecules. All STM images were obtained at  $\sim 5 \, \text{K}$  (20 mV and 0.2 nA). The scale bars are (b) 0.5 nm and (c) 5.0 nm, respectively. Reproduced with permission from [61]. Copyright 2017 American Chemical Society.

# 3.2. Discussion of the reaction mechanism in terms of interfacial electronic structure

To elucidate the photodissociation mechanism of  $(CH_3S)_2$  molecules on the Ag(111) and Cu(111) surfaces, we carried out periodic DFT calculations [61]. The atomically resolved STM images reveal the adsorption site of the molecules: the molecular center is positioned above bridge sites, and two S atoms are located at the on-top sites of adjacent metal atoms (Fig. 6(a)). The local density of states (LDOS) of an  $(CH_3S)_2$  molecule and the projected density of states (PDOS) of the three p-states of its two S atoms calculated on

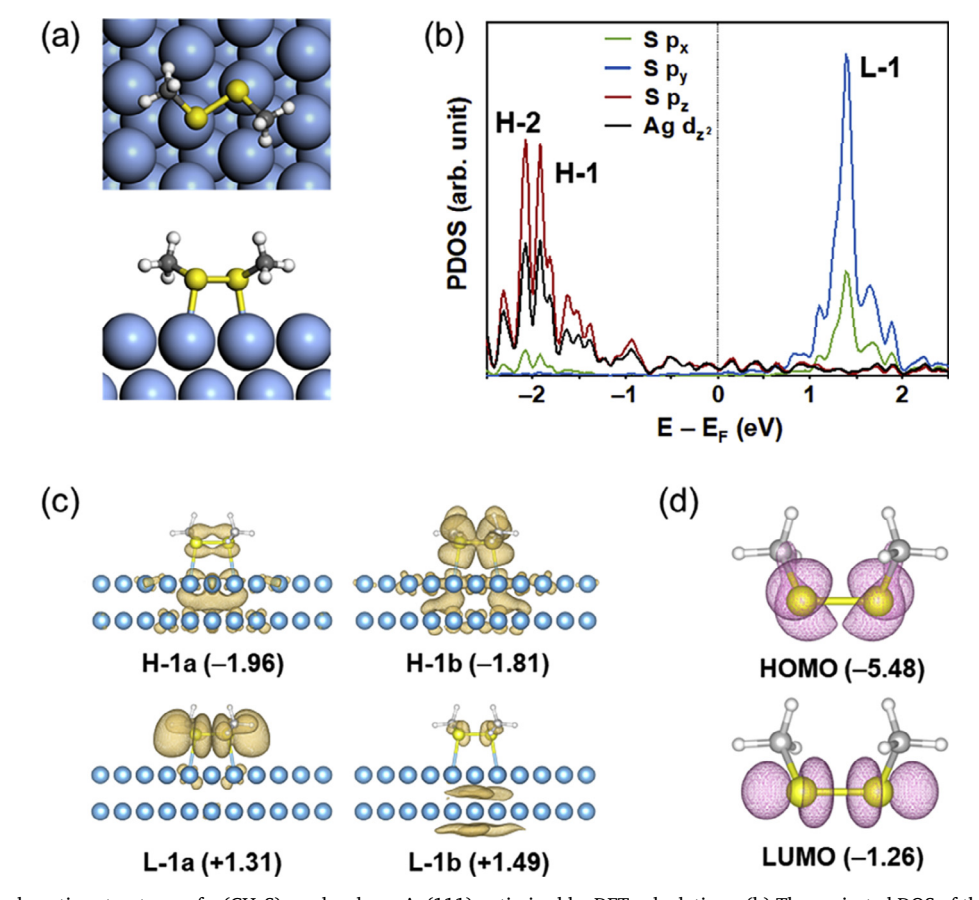


Fig. 6. (a) The adsorption structures of a  $(CH_3S)_2$  molecule on Ag(111) optimized by DFT calculations. (b) The projected DOS of three p-states on S atoms in a  $(CH_3S)_2$  molecule and  $d_z^2$ -state of two metal atoms that are underneath the S atoms and directly interact with the molecule on Ag(111). (c) The spatial distribution (isovalue =  $0.0005 e/bohr^3$ ) of the molecular frontier states nearest to  $E_F$  for an isolated  $(CH_3S)_2$  molecule on Ag(111). (d) The spatial distribution (isovalue =  $0.01 e/bohr^3$ ) of the HOMO and LUMO orbitals in the gas phase  $(CH_3S)_2$ . Reproduced with permission from [61]. Copyright 2017 American Chemical Society.

the metal surfaces indicate that the S p-states mainly contribute to the first prominent LDOS peaks of  $(CH_3S)_2$  nearest  $E_F$  [61]. The occupied and unoccupied molecular states near the  $E_F$  are dominantly composed of the S  $p_z$ -state, and S  $p_x$ - and  $p_y$ -states, respectively (Fig. 6(b)). The spatial distributions of molecular frontier states for  $(CH_3S)_2$  adsorbed on the Ag(111) surfaces indicate that H-1 state  $(\sim -1.9 \text{ eV})$  consist of  $\pi$ -bonding orbital along the S-S bond  $(\pi_{SS})$  and nonbonding lone-pair type orbitals on the S atoms  $(n_S)$ , and L-1 state  $(\sim +1.4 \text{ eV})$  is characterized by the antibonding orbital localized on the S - S bond  $(\sigma^*_{SS})$  (Fig. 6(c)). The H-1b and L-1 states are very similar to the HOMO and LUMO states of  $(CH_3S)_2$  in the gas phase, respectively (Fig. 6(d)). The appearance of H-1a state in the frontier region can be understood by enhancement of molecular planarity due to the adsorption on the surface, where the dihedral angle of 82.8° along the S-S bond in the gas phase increases to 134.2° (126.7°) on Ag (Cu) surface. The spatial distributions of electronic states on Cu(111) are almost identical to those of the electronic states observed on Ag(111).

In the gas-phase reaction, dissociation of the S–S bond of  $(CH_3S)_2$  predominantly occurs with 248 nm ( $\sim$ 5.0 eV) light through the direct electronic excitation from  $n_S$  to  $\sigma^*_{SS}$  [84–87]. Considering the remarkable similarity of the frontier states on the metal substrates to the molecular orbitals of the gas phase  $(CH_3S)_2$  (Fig. 6(c, d)), the photodissociation of the S–S bond on the metal surface can also occur through direct electronic excitation between the frontier electronic states ( $n_S \rightarrow \sigma^*_{SS}$ ). The computationally estimated energy gaps for the excitation pathway ( $n_S \rightarrow \sigma^*_{SS}$ ) are 3.12–3.30 eV (376–397 nm) and 2.27–2.51 eV (494–546 nm) on Ag(111) and on Cu(111), respectively. Although the conventional DFT calculations cannot exactly describe the HOMO-LUMO gap due to the limitations of neglecting exact Hartree-Fock exchange, the computational results not only describe the reduction of the energy gap from the HOMO-LUMO gap of gas phase  $(CH_3S)_2$  but also provide a way to qualitatively explain the experimental results in which the threshold energy for photodissociation on Cu(111) was found to be lower than that on Ag(111) (Fig. 4(c)). Moreover, the reduced energy gap due to hybridization, i.e., coupling between the electronic states of adsorbate and metal substrate, enables photodissociation by visible light.

The alignment of molecular frontier states with respect to the metal-states of the two metal atoms underneath the S atoms reveals the degree of interfacial hybridization between molecular orbitals and metal states, for which the energy region corresponds to the edge of Ag 4d state. Fig. 6(b) shows that the HOMO-derived states align well with the  $d_z^2$ -state of the two Ag atoms underneath the S atoms, but there is no significant distribution of the metal-state in the unoccupied region. The same tendency was also observed on the Cu(111) surface. The spatial distribution of molecular orbitals for (CH<sub>3</sub>S)<sub>2</sub> adsorbed on the metal clearly represents the strong and weak interfacial hybridization between the molecule and the metal at HOMO- and LUMO-derived states, respectively (Fig. 6(c)). In particular, the weakly hybridized electronic structure in the unoccupied region may suppress the rapid relaxation of the excited states. We thus conclude that the weak interactions between the frontier molecular orbitals and the metal states, especially in the unoccupied region, extend the excited-state lifetimes sufficiently to induce photodissociation.

The experimentally observed photodissociation by visible light can be explained by reduction of the optical energy gap of  $(CH_3S)_2$  due to the hybridization between electronic states of adsorbate and metal substrate, in which the molecular frontier states with less overlap with the metal substrate enables a reaction pathway for the photodissociation of adsorbate.

# 4. Plasmon chemistry of dimethyl disulfide

Most papers related to plasmon-induced chemical reactions have been published since 2010, and influential review papers have also been recently published [36-39]. In this section, we describe the excitation mechanisms of the plasmon-induced chemical reaction of the  $(CH_3S)_2$  molecules on the basis of the STM investigation of single-molecule reaction. Furthermore, we discuss the reaction pathways in terms of the electronic structures of the molecules adsorbed on the metal surfaces.

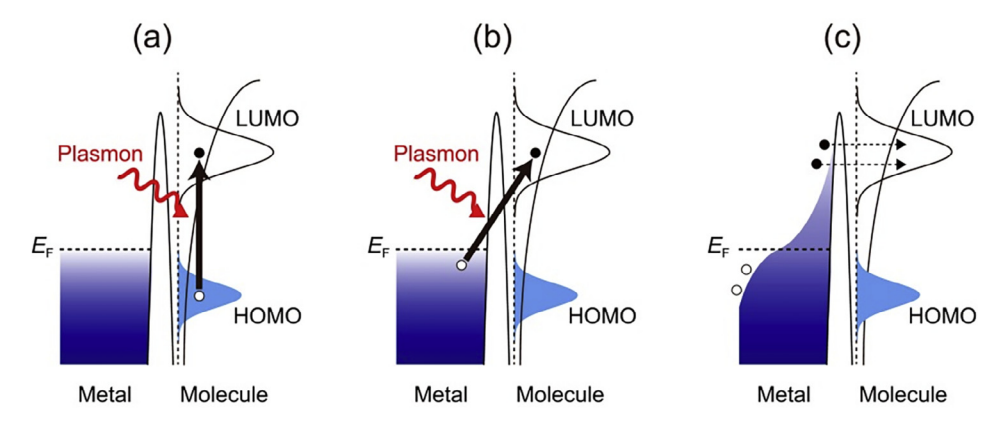


Fig. 7. Excitation mechanisms proposed for plasmon-induced chemical reactions. (a) Direct intramolecular excitation mechanism. (b) Charge-transfer mechanism. The electrons are resonantly transferred from the metal to the unoccupied states of the molecule. (c) Indirect hot-electron transfer mechanism. Hot electrons generated via nonradiative decay of the plasmon transferred to the unoccupied states to form the TNI states of the molecule. Black and white dots indicate electrons and holes, respectively.

## 4.1. Excitation mechanisms and reaction profiles of plasmon-induced chemical reactions

The possible excitation mechanisms of the plasmon-induced chemical reactions are illustrated in Fig. 7. The direct intramolecular excitation mechanism (Fig. 7(a)) and the charge-transfer mechanism (Fig. 7(b)) are the same concepts as the resonance Raman enhancement mechanism and charge-transfer resonance enhancement mechanism in SERS, respectively [88]. In the direct intramolecular excitation mechanism (Fig. 7(a)), the transition from the HOMO to the LUMO of the molecules is resonantly excited by the plasmon having the same energy as the HOMO-LUMO gap. In the charge-transfer mechanism (Fig. 7(b)), the plasmon induces resonant charge-transfer from the metal states near the Fermi level to the LUMO. The enhancement of SERS intensities of molecules such as pyridines, pyrazine and p-aminothiophenol adsorbed on Ag, Cu, and Au surfaces were explained by the charge-transfer mechanism, and the Raman intensity became highest when the energy of the plasmon is same as the energy difference between the Fermi level and the LUMO [89]. The charge-transfer mechanism was also applied to describe the plasmon-induced chemical transformation of methylene blue adsorbed on Ag nanocubes [54]. Although the interaction between the plasmon and molecules has long been enthusiastically discussed as a chemical enhancement mechanism in the field of SERS, a complete explanation of the enhancement mechanism has not been obtained due to complicated experimental conditions such as non-uniform surface of metal nanoparticles, aggregations of nanoparticles, and less information of electronic structures of adsorbed molecules [88].

In addition to these two mechanisms, in plasmon chemistry, most studies have applied the indirect hot-electron transfer mechanism (Fig. 7(c)) to explain the reactions [36–39]. The hot electrons generated by nonradiative decay of the plasmon transfer from the metal to the molecule, which leads to the TNI state of the adsorbed molecule. The plasmon-induced dissociations of  $O_2$  [44,46] and  $H_2$  [47,52] molecules were explained by a mechanism in which the dissociation reactions proceed through vibrational excitation after the formation of the TNI states.

The wavelength dependence of the plasmon-induced dissociation rate (or yield) provides mechanistic insights. The dissociation rate reported for  $H_2$  molecules adsorbed on Au nanoparticles/ $SiO_2$  photocatalyst exhibits excellent agreement with the calculated absorption spectrum of the Au/ $SiO_2$  photocatalyst (Fig. 8 (a,b)) [52]. This indicates that the indirect hot-electron transfer mechanism governs this dissociation reaction, because the dissociation rate is influenced by the energy distribution of the hot electrons, which is sensitive to the electronic band structure of metals [90].

In our recent study, the plasmon-induced dissociation of the S–S bond in the (CH<sub>3</sub>S)<sub>2</sub> molecules adsorbed on Ag(111) and Cu(111) surfaces was induced by the plasmon optically excited in the nanogap between the Ag tip and the metal surface (Fig. 9) [62]. The Ag tips with the same cone angle ( $\theta$ ) and curvature radius (r) were selected for use on the basis of SEM images ( $\theta$  = 15 ± 1.2° and r = 58 ± 4.9 nm) (Fig. 9 (b,c)), because the plasmonic properties strongly depend on the tip shape. The Ag tip was positioned over the bare metal surface under the tunneling condition ( $V_s$  = 20 mV and  $I_t$  = 0.2 nA) during light irradiation (Fig. 9(d)). Tunneling electrons at a bias of 20 mV cannot excite vibrational modes related to any kinds of reactions and molecular motions [91,92]. The spatial distribution of the (CH<sub>3</sub>S)<sub>2</sub> molecules on Ag(111) after the excitation of the plasmon with 532 nm light revealed that the molecules near the tip position were preferentially dissociated due to the plasmon (Fig. 9(d)). Notably, other reactions, such as rotation or desorption, were not observed. The dissociation rate constant (k) was obtained from time dependence of the dissociation ratio ( $N/N_0$ ) (( $\ln(N/N_0)$ ) = -kt). From comparison of the lateral distance dependence of k with the simulated lateral profile of electromagnetic field intensity in the nanogap ( $E_{\rm gap}$ ) (Fig. 9(e)), the plasmon-induced dissociation has a strong correlation with the electric field intensity of the plasmon.

Maksymovych et al reported nonlocal dissociation of the  $(CH_3S)_2$  molecules on Au(111) induced by injecting tunneling electrons from a W tip [93]. The threshold bias voltages of the nonlocal dissociation was reported as ~1.4 eV. The nonlocal dissociation was explained by lateral propagation of hot electrons injected from the STM tip, and excitation mechanisms by electric field effect and field-emission current were excluded. The spatial distribution of the reacted molecules became larger as the intensity of tunneling current increased (from 10 to 100 nm in diameter), which supported lateral propagation of hot electrons. In contrast to the nonlocal dissociation induced by hot electrons from the STM tip, the spatial distribution of dissociated molecules was determined by the lateral distribution of the electric field of the plasmon (Fig. 9(e)).

Fig. 8(c) shows the wavelength dependence of the dissociation yield on Ag(111) obtained in the 10-nm-diameter circle under the tip. The wavelength at the maximum intensity and the threshold wavelength of the yield are  $\sim$ 532 nm ( $\sim$ 2.33 eV) and  $\sim$ 780 nm ( $\sim$ 1.59 eV), respectively, which are longer than those of photodissociation. The spectral shape of the yield is similar to that of the simulated electric field intensity in the nanogap at the wavelengths where photodissociation occurs. Furthermore, the maximum intensity of the yield (Fig. 8(c)) was  $\sim$ 400 times higher than that of the photodissociation yield (Fig. 4(c)). These results indicate that the plasmon was an efficient excitation source. Moreover, the overall shapes of the spectra of the yield also reflected the spectral shape of the photodissociation yield, that is, the energy distribution of the DOSs for both the HOMO- and LUMO-derived molecular states. We therefore conclude that the plasmon efficiently induces and enhances the dissociation reaction through the same reaction pathway as photodissociation ( $n_s \rightarrow \sigma^*_{SS}$ ) by the direct intramolecular excitation mechanism (Fig. 7(a)).

The plasmon-induced dissociation was also induced at longer wavelengths where photodissociation never occurred, as indicated in the tail of the spectrum (Fig. 8(c)). To explain this low-efficiency reaction in the long-wavelength region, both the direct intramolecular excitation from the molecular orbitals in-gap states near the  $E_{\rm F}$  to  $\sigma^*_{\rm SS}$  (MO<sub>in-gap</sub>  $\rightarrow \sigma^*_{\rm SS}$ ) and the charge transfer from the metal state near the  $E_{\rm F}$  to  $\sigma^*_{\rm SS}$  should be taken into account. However, it is difficult to distinguish them based on analysis of the wavelength-dependent reaction yield. A more detailed discussion was provided in our previous study [62].

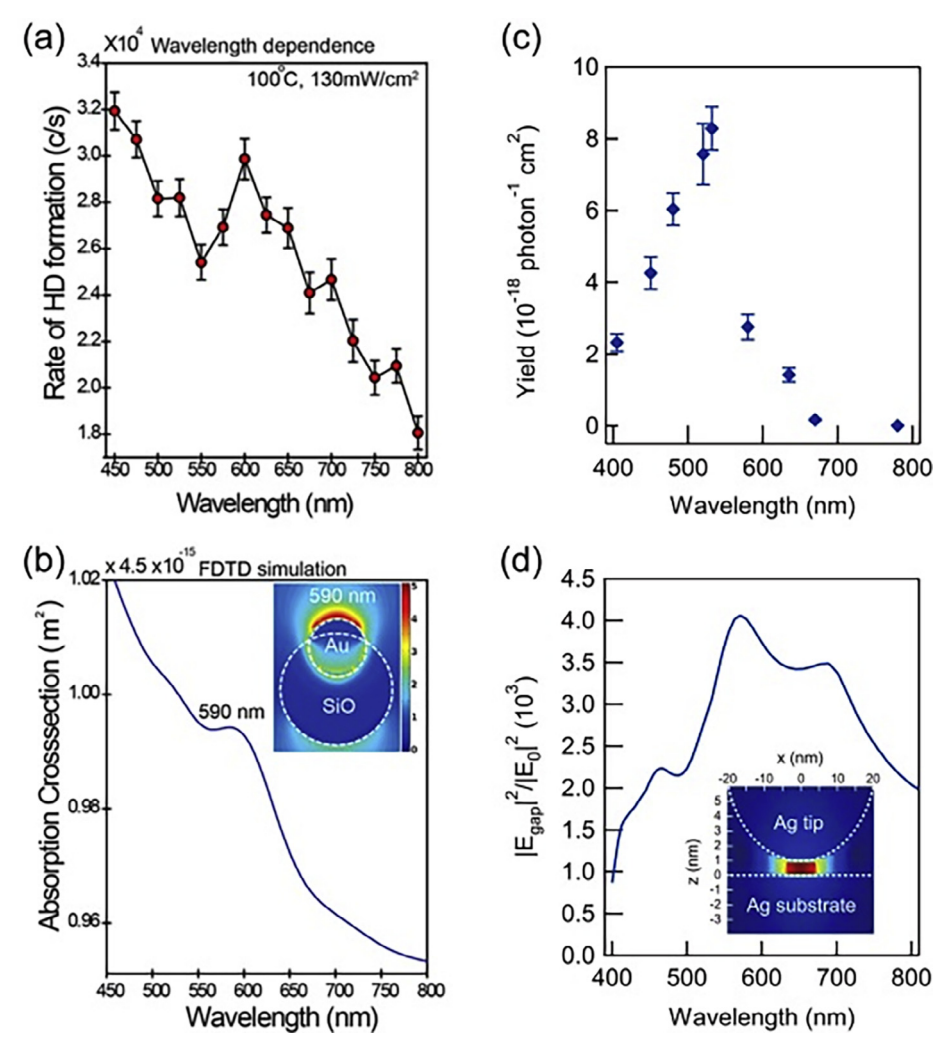


Fig. 8. (a) Wavelength dependence of the rate of HD formation at  $100\,^{\circ}$ C using 1% Au/SiO<sub>2</sub>. (b) Simulated absorption cross section of the Au/SiO photocatalyst. The simulation model is a 10-nm Au nanoparticle 75% embedded into a 40-nm SiO<sub>2</sub> nanoparticle. Inset shows the local electric field near the Au/SiO photocatalyst. (c) Wavelength dependence of plasmon-induced dissociation yield of (CH<sub>3</sub>S)<sub>2</sub> molecules on Ag(111). (d) Wavelength dependence of calculated electric field intensity for a 1-nm gap between a Ag tip and the Ag substrate under p-polarized light. The simulated point is  $z=0.1\,\text{nm}$  above the substrate surfaces and  $z=0\,\text{nm}$ . (a, b) Reproduced with permission from [52]. Copyright 2014 American Chemical Society. (c, d) Reprinted with permission from *Science* (http://www.aaas.org), [62]. Copyright 2018 American Association for the Advancement of Science.

# 4.2. STM investigation of single-molecule reaction induced by a plasmon

The STM allows real-space analyses of the plasmon-induced chemical reaction as described in Section 4.1. In addition, the reaction time of a single molecule is provided by the current trace measurement, as explained in Section 2.2, which gives insights into the elementary reaction pathways that cannot be accessed by conventional spectroscopies and the analysis of the wavelength dependence of the yield. Fig. 10(a) shows an experimental scheme of the current trace when the STM tip was positioned over the  $(CH_3S)_2$  molecule on Ag(111) under light irradiation. A one-time change in tunneling current indicates that one kind of molecular motion or reaction happened. In the case of the  $(CH_3S)_2$  molecule, a sudden drop in the current was caused by the dissociation of the molecule (Fig. 10(b)).

The STM can also reveal the reaction pathways initiated from the TNI states formed by electron transfer from the metal to the molecule via the IET process. Both the hot electrons of the plasmon and the tunneling electrons inelastically transfer to the unoccupied molecular orbitals to form the TNI states. The reaction pathways initiated from the TNI states in the same energy regions should be the same regardless of the origin of the excitation source, because both the hot electrons and tunneling electrons had a broad energy distribution from  $E_F$  to the energy of the plasmon ( $E_F + E_{LSP}$ ) and the applied sample bias voltage ( $E_F + e^- V_{bias}$ ), respectively.

Rotation and dissociation of the  $(CH_3S)_2$  molecule on Ag(111) were induced through vibrational excitation by injecting the tunneling electrons at energies higher than  $\sim 0.28$  and  $\sim 0.36$  eV, respectively (Fig. 11(a-c)). Dissociation occurred through

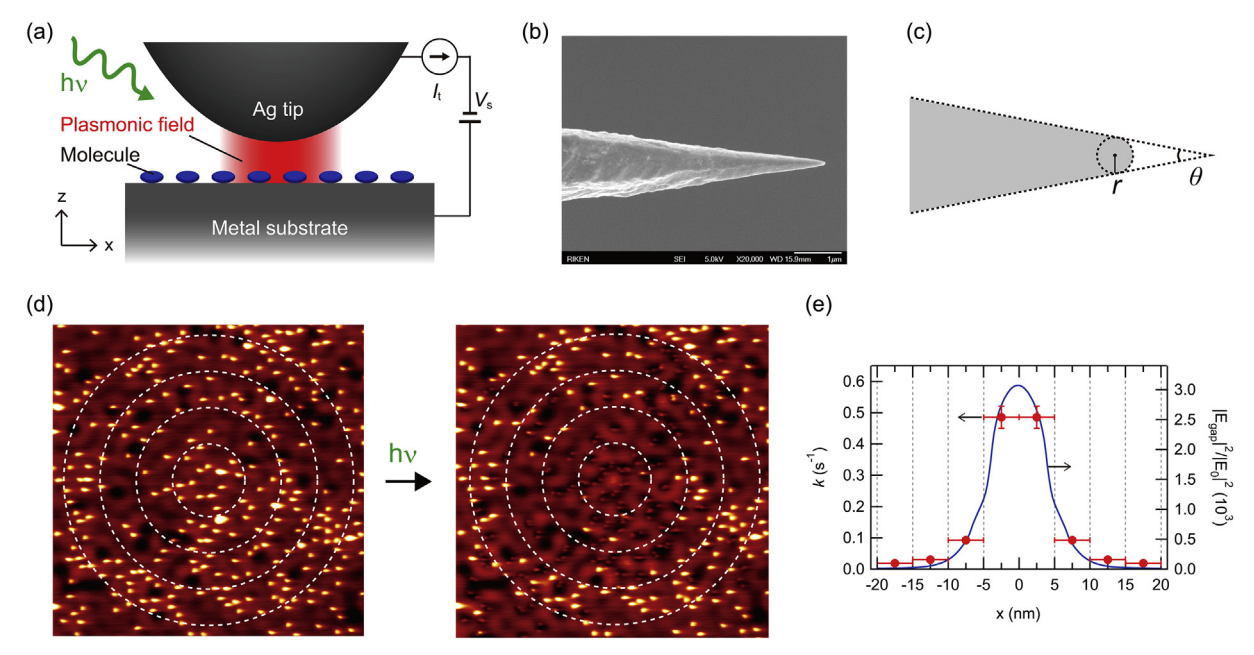


Fig. 9. (a) Schematic illustration of the experiment for the plasmon-induced chemical reaction in the nanogap between a Ag tip and a metal substrate. The tip was positioned over the metal surface during light irradiation with the feedback loop turned on to maintain the gap distance.  $V_s$  and  $I_t$  are kept at 20 mV and 0.2nA. (b) An SEM image of a typical Ag tip used in this study. The scale bar is 1 μm. (c) Schematic illustration of the Ag tip drawn from the SEM images. θ and r estimated from the SEM image were used for calculation of  $E_{\rm gap}$ . (d) Topographic STM images of the (CH<sub>3</sub>S)<sub>2</sub> molecule adsorbed on Ag(111) before and after irradiation with p-polarized light at 532 nm ( $\sim$ 7.6 × 10<sup>17</sup> photons cm<sup>-2</sup> s<sup>-1</sup>, 2 s) ( $V_s$  = 20 mV,  $I_t$  = 0.2nA, 43 × 43 nm<sup>2</sup>). The tip was positioned at the center of the dotted circle during light irradiation. (e) k obtained at four areas depicted with 10 nm wide concentric rings (532 nm light,  $\sim$ 5.9 × 10<sup>16</sup> photons cm<sup>-2</sup> s<sup>-1</sup>). Each data point is the average of six trials. Solid curve is the calculated lateral profile of  $E_{\rm gap}$  with the Ag tip (θ = 15°, r = 60 nm) under 533 nm light. x = 0 nm corresponds to the center of the tip. Reprinted with permission from *Science* (http://www.aaas.org), [62]. Copyright 2018 American Association for the Advancement of Science.

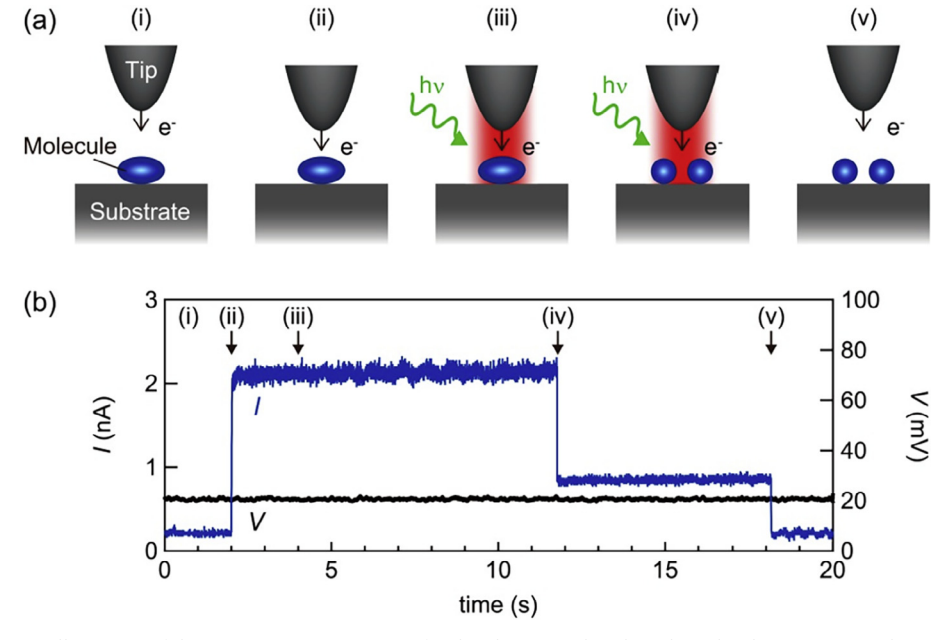


Fig. 10. (a) Schematic illustration of the current trace experiment for the plasmon-induced single molecule reaction. (i) The Ag tip was positioned above the molecule (V = 20 mV and I = 0.2 nA). (ii) The fixed gap resistance (V = 20 mV and I = 2.0 nA) was applied and the feedback loop was turned off to maintain the tip height. (iii) Light irradiation started. (iv) The light was turned off and the feedback loop was turned on, and (v) the tip height returned to the initial position. (b) Current trace for detecting the dissociation event for the single ( $CH_3S_2$ ) molecule on  $CH_3S_2$  molecule on  $CH_3S_3$  mol

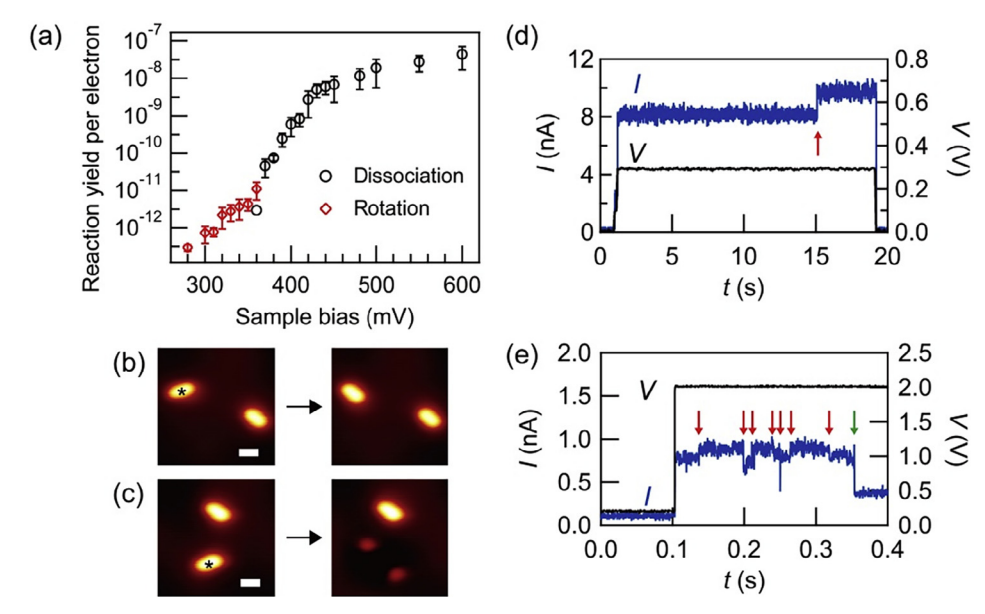


Fig. 11. IET-induced reactions in the dark. (a) Action spectrum for the rotation and dissociation of the  $(CH_3S)_2$  molecules induced by injecting tunneling electrons from the STM tip. (b, c) STM images of the molecule before and after the IET-induced (b) rotation and (c) dissociation. The tip position is indicated by the \* in the STM image. The scale bars in the STM images in (b, c) are 0.5 nm. (d, e) Current trace was measured on the molecules with the feedback loop turned off. The tunneling conditions were (d)  $V = 0.30 \, \text{V}$  and  $I = 8.0 \, \text{nA}$ , and (e)  $V = 2.0 \, \text{V}$  and  $I = 1.0 \, \text{nA}$ . The current changes indicated by red and green arrows correspond to rotation and dissociation, respectively. Reprinted with permission from *Science* (http://www.aaas.org), [62]. Copyright 2018 American Association for the Advancement of Science. (For interpretation of the references to colour in this figure legend, the reader is referred to the web version of this article.)

vibrational excitation of the C–H stretch mode [91] and a combination of the C–H stretch and the S–S stretch modes [92]. Small changes in the current followed by its sudden drop resulted from dissociation accompanied by rotation (Fig. 11(d, e)). This result reveals that the energy of the TNI states was dissipated to the vibrationally excited states according to the non-dissociative potential energy surface (Fig. 12(a)), which resulted in both rotation and dissociation of ( $CH_3S$ )<sub>2</sub>. Thus, the IET process through vibrational excitation at the lower-energy region is always included in the reaction pathway when the energy of electrons is higher than the vibrational energies of the ground state.

The current trace measured for the single-molecule reaction induced by the plasmon exhibited only a one-time change due to dissociation and is not accompanied by rotational motion prior to dissociation (Fig. 10). This excluded the hot-electron-mediated process as an elementary pathway for the plasmon-induced dissociation of  $(CH_3S)_2$ . By considering the results of the wavelength dependence of dissociation yield (Section 4.1) and the DFT calculations (Section 3.3), we concluded that the plasmon-induced dissociation of  $(CH_3S)_2$  occurred through the direct dissociation pathway from neutral excited states generated by direct intramolecular excitation (Fig. 12(a)).

# 4.3. Reaction pathways of the plasmon-induced chemical reactions

In the indirect hot-electron transfer mechanism (Fig. 7(c)), the hot electrons of the plasmon do not have a specific energy but have a broad energy distribution from  $E_F$  to the energy of the plasmon ( $E_F + E_{LSP}$ ). Therefore, they can induce all possible reaction pathways initiated from the TNI states. The non-dissociative TNI states (Fig. 12(b)) resulting in rotational motion are always included in the reaction pathway when the electrons are broadly distributed from the Fermi level to the upper energy level, which is higher than the vibrational energies of the ground state.

In the charge-transfer mechanism (Fig. 7(b)), the electrons with a specific energy ( $E_{\rm e} = \Delta({\rm LUMO} - E_{\rm F})$ ) are resonantly transferred from the Fermi level to the LUMO states, resulting in the formation of negative ion states (Fig. 12(c)). The reaction pathway through this excited state cannot be separated from the reaction through vibrational excitation induced in the lower-energy region ( $E_{\rm e} < \Delta({\rm LUMO} - E_{\rm F})$ ) (Fig. 12(b)) in the STM experiment due to the broad energy distribution of the tunneling electrons. In other words, we cannot determine the shape of the potential energy surface, non-dissociative (Fig. 12(c)-(i)) or dissociative (Fig. 12(c)-(ii)) in the charge-transfer mechanism. In the plasmon-induced dissociation of (CH<sub>3</sub>S)<sub>2</sub>, the charge transfer from near the Fermi level to the LUMO ( $\sigma^*_{\rm SS}$ ) states (Fig. 7(b)) as well as the direct intramolecular excitation (Fig. 7(a)) is a possible excitation mechanism. The computationally estimated energy gaps between  $E_{\rm F}$  and  $\sigma^*_{\rm SS}$  are about 1.0–2.0 eV and 0.8–1.5 eV on Ag(111) and Cu(111), respectively. Thus, the charge transfer can also contribute to the tails of the  $Y_{\rm LSP}$ - $\lambda$  spectra in the low energy region only if the potential energy surface is dissociative (Fig. 12(c)-(ii)).

In consequence, the indirect hot-electron transfer mechanism (Fig. 7(c)) is definitively ruled out by our precisely controlled STM experiment. The plasmon-induced dissociation of  $(CH_3S)_2$  is explained by the direct intramolecular excitation mechanism (Fig. 7(a))

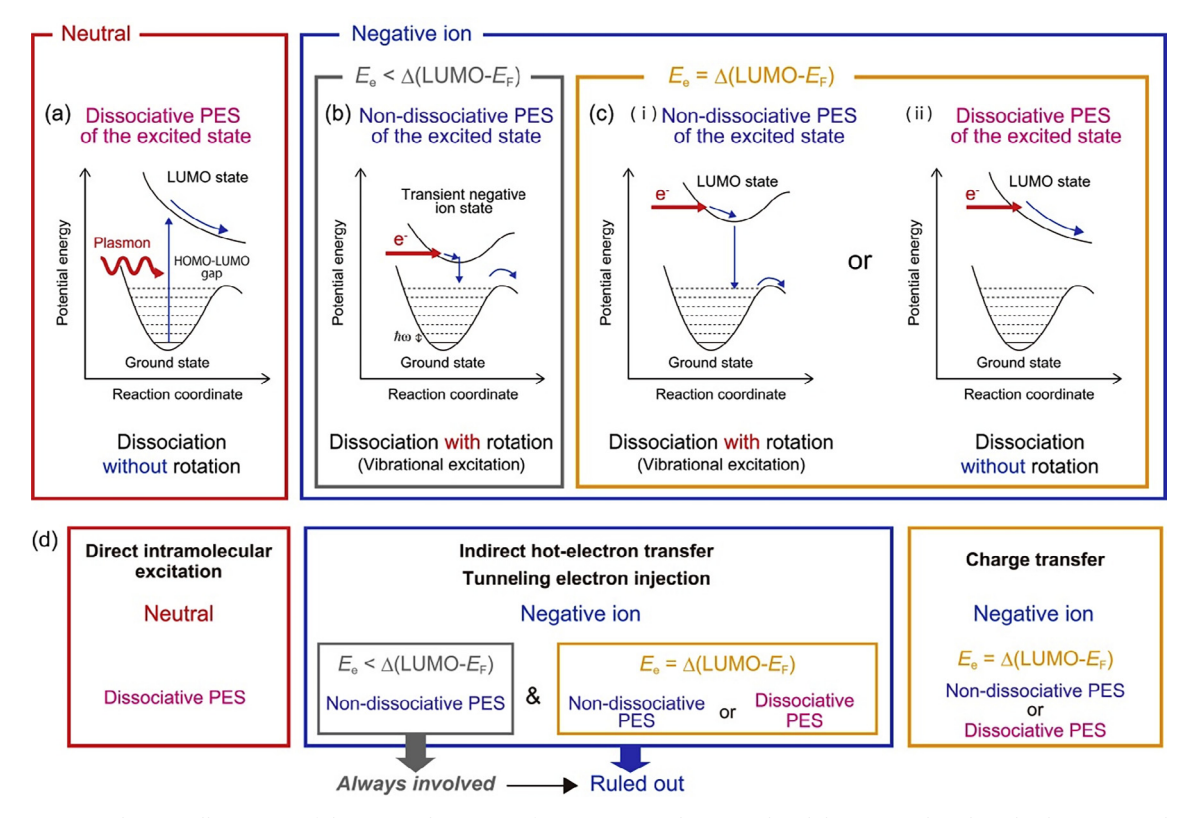


Fig. 12. (a–c) Schematic illustrations of the potential energy surfaces (PES). (a) Plasmon-induced dissociation based on the direct intramolecular excitation mechanism. Dissociation occurs from the neutral excited states. (b, c) Reactions initiated from the TNI states formed by electron transfer from the metal to the molecule. (b) The energy of the electrons ( $E_e$ ) is less than the gap between the LUMO and the Fermi level ( $\Delta$  (LUMO –  $E_F$ ). The potential energy surface of the excited state is (i) non-dissociative or (ii) dissociative. (d) Relation between the excitation mechanisms and the potential energy surfaces of the excited states.

along the potential energy surface shown in Fig. 12(a). Notably, weak hybridization between the LUMOs of  $(CH_3S)_2$  and the metal states allows access to the dissociative potential energy surface from the neutral excited states, which was theoretically predicted for the photodissociation of  $(CH_3S)_2$  molecules in the gas phase [87]. In addition, the charge-transfer mechanism would also contribute to the reaction if the potential energy surface of the excited state is dissociative (Fig. 11(c)–(ii)). In our STM studies, however, we cannot quantitatively evaluate the contribution of the charge-transfer mechanism.

# 5. Concluding remarks

The STM combined with optical excitation provides real-space information on photochemical reactions and plasmon-induced chemical reactions. Visible-light-induced photodissociation of the S–S bond in  $(CH_3S)_2$  molecules adsorbed on Ag(111) and Cu(111) surfaces was explored with the STM. The experimental results combined with DFT calculations of the frontier electronic states revealed that photodissociation on the metal surfaces occurred through direct intramolecular excitation  $(n_S \to \sigma^*_{SS})$ . The photodissociation pathway available for visible light became accessible because the hybridization between the molecular orbitals and the metal substrate causes not only the reduction of the optical energy gap into the range of visible light but also the generation of LUMO states with less overlap with the metal substrate.

Plasmon-induced dissociation of the S–S bond in  $(CH_3S)_2$  on the metal surfaces was also achieved in the nanogap between the STM tip and the metal substrate. The STM investigation of a single-molecule reaction revealed that the plasmon-induced dissociation of the molecule with the electronic states less hybridized with the metals occurred principally by the direct intramolecular excitation to the LUMO state  $(\sigma^*_{SS})$ . The STM combined with optical excitation allows us to obtain fruitful mechanistic insights into the chemical reactions induced by photons and plasmons, which cannot be gained by conventional spectroscopies.

# Acknowledgements

The present work was supported in part by a Grant-in-Aid for Scientific Research (A) (15H02025), a Grant-in-Aid for Young Scientists (B) (16K17862), and the RIKEN postdoctoral researchers (SPDR) program. J.J. acknowledges the financial support of the National Research Foundation under the Next Generation Carbon Upcycling Project (grant 2017M1A2A2043144) of the Ministry of

Science and Information and Communication Technology, Republic of Korea. H.U. was supported by Ministry of Education, Culture, Sports, Science and Technology Grants-in-Aid for Scientific Research (KAKENHI) grant C-2539000, which allows him to continue to work after retirement from the University of Toyama. M.T. acknowledges support from a grant from the NSF (CHE-1800236). We are grateful for the use of the HOKUSAI-GreatWave supercomputer system of RIKEN.

#### References

- [1] C.D. Lindstrom, X.Y. Zhu, Photoinduced electron transfer at molecule-metal interfaces, Chem. Rev. 106 (2006) 4281–4300.
- [2] C. Frischkorn, M. Wolf, Femtochemistry at metal surfaces: Nonadiabatic reaction dynamics, Chem. Rev. 106 (2006) 4207-4233.
- [3] L. Hanley, X.C. Guo, J.T. Yates, Photolysis of chemisorbed dioxygen on Pd(111): Dependence on photon energy, J. Chem. Phys. 91 (1989) 7220-7227.
- [4] Z.M. Liu, S.A. Costello, B. Roop, S.R. Coon, S. Akhter, J.M. White, Surface Photochemistry: 6. CH<sub>3</sub>Br on Pt(111), J. Phys. Chem. 93 (1989) 7681–7688.
- [5] X.Y. Zhu, S.R. Hatch, A. Campion, J.M. White, Surface photochemistry. II. Wavelength dependences of photoinduced dissociation, desorption, and rearrangement of O<sub>2</sub> on Pt(111), J. Chem. Phys. 91 (1989) 5011–5020.
- [6] S.K. So, R. Franchy, W. Ho, Photodesorption of NO from Ag(111) and Cu(111), J. Chem. Phys. 95 (1991) 1385–1399.
- [7] Z.C. Ying, W. Ho, Photodissociation of adsorbed Mo(CO)<sub>6</sub> induced by direct photoexcitation and hot electron attachment. II. Physical mechanisms, J. Chem. Phys. 94 (1991) 5701–5714.
- [8] S.K. So, W. Ho, Resonant photodissociation of Mo(CO)<sub>6</sub> adsorbed on graphite and Ag(111), J. Chem. Phys. 95 (1991) 656-671.
- [9] S.R. Hatch, X.Y. Zhu, J.M. White, A. Campion, Photoinduced Pathways to Dissociation and Desorption of Dioxygen on Ag(110) and Pt(111), J. Phys. Chem. 95 (1991) 1759–1768.
- [10] X.Y. Zhu, J.M. White, M. Wolf, E. Hasselbrink, G. Ertl, Polarization probe of excitation mechanisms in surface photochemistry, Chem. Phys. Lett. 176 (1991) 459–466.
- [11] X.Y. Zhu, J.M. White, The role of direct and substrate excitation in ultraviolet photolysis of phosgene on Pt(111), J. Chem. Phys. 94 (1991) 1555-1563.
- [12] C.R. Flores, X.Y. Zhu, J.M. White, Photodissociation of Phosgene on Pd(ll1) at 193 nm, J. Phys. Chem. 95 (1991) 9431–9436.
- [13] J. Kiss, D.J. Alberas, J.M. White, Surface-aligned photoreaction of DBr with C<sub>2</sub>H<sub>4</sub> on Pt(111), J. Am. Chem. Soc. 114 (1992) 10486–10492.
- [14] W.D. Mieher, W. Ho, Bimolecular surface photochemistry: Mechanisms of CO oxidation on Pt(111) at 85 K, J. Chem. Phys. 99 (1993) 9279–9295.
- [15] St. J. Dixon-Warren, E.T. Jensen, J.C. Polanyi, Photochemistry of adsorbed molecules. XI. Charge-transfer photodissociation and photoreaction in chloromethanes on Ag(111), J. Chem. Phys. 98 (1993) 5938–5953.
- [16] K. Watanabe, K. Sawabe, Y. Matsumoto, Adsorbate-localized excitation in surface photochemistry: methane on Pt(111), Phys. Rev. Lett. 76 (1996) 1751–1754.
- [17] R.T. Kidd, D. Lennon, S.R. Meech, Comparative study of the primary photochemical mechanisms of nitric oxide and carbonyl sulfide on Ag(111), J. Phys. Chem. B 103 (1999) 7480–7488.
- [18] J. Lee, S. Ryu, J.S. Ku, S.K. Kim, Charge transfer photodissociation of phenol on Ag(111), J. Chem. Phys. 115 (2001) 10518–10524.
- [19] H. Petek, S. Ogawa, Femtosecond time-resolved two-photon photoemission studies of electron dynamics in metals, Prog. Surf. Sci. 56 (1997) 239-310.
- [20] M. Wolf, A. Hotzel, E. Knoesel, D. Velic, Direct and indirect excitation mechanisms in two-photon photoemission spectroscopy of Cu(111) and CO/Cu(111), Phys. Rev. B 59 (1999) 5926–5935.
- [21] H. Petek, M.J. Weida, H. Nagano, S. Ogawa, Real-time observation of adsorbate atom motion above a metal surface, Science 288 (2000) 1402-1404.
- [22] W. Berthold, P. Feulner, U. Höfer, Laser-induced desorption of Ar from Cu(100) probed by two-photon photoemission spectroscopy of image-potential states, Surf. Sci. 548 (2004) L13–L20.
- [23] S. Ryu, J. Chang, S.K. Kim, Interfacial electron dynamics and hot-electron-driven surface photochemistry of carbon tetrachloride on Ag(111), J. Chem. Phys. 123 (2005) 114710.
- [24] A.B. Zrimsek, N. Chiang, M. Mattei, S. Zaleski, M.O. McAnally, C.T. Chapman, A. Henry, G.C. Schatz, R.P. Van Duyne, Single-molecule chemistry with surface-and tip-enhanced Raman spectroscopy, Chem. Rev. 177 (2017) 7583–7613.
- [25] T. Hartman, C.S. Wondergem, N. Kumar, A. van den Berg, B.M. Weckhuysen, Surface- and tip-enhanced Raman spectroscopy in catalysis, J. Phys. Chem. Lett. 7 (2016) 1570–1584.
- [26] Y.F. Huang, H.P. Zhu, G.K. Liu, D.Y. Wu, B. Ren, Z.Q. Tian, When the signal is not from the original molecule to be detected: chemical transformation of para-aminothiophenol on Ag during the SERS measurement, J. Am. Chem. Soc. 132 (2010) 9244–9246.
- [27] H.Y. Zhu, X.B. Ke, X.Z. Yang, S. Sarina, H.W. Liu, Reduction of nitroaromatic compounds on supported gold nanoparticles by visible and ultraviolet light, Angew. Chem. Int. Ed. 49 (2010) 9657–9661.
- [28] M. Sun, Y. Huang, L. Xia, X. Chen, H. Xu, The pH-controlled plasmon-assisted surface photocatalysis reaction of 4-aminothiophenol to p, p '-dimercaptoazo-benzene on Au, Ag, and Cu colloids, J. Phys. Chem. C 115 (2011) 9629–9636.
- [29] L.L. Kang, P. Xu, B. Zhang, H.H. Tsai, X.J. Han, H.L. Wang, Laser wavelength- and power-dependent plasmon-driven chemical reactions monitored using single particle surface enhanced Raman spectroscopy, Chem. Comm. 49 (2013) 3389–3391.
- [30] Z. Zhang, T. Deckert-Gaudig, P. Singh, V. Deckert, Single molecule level plasmonic catalysis a dilution study of p-nitrothiophenol on gold dimers, Chem. Comm. 51 (2015) 3069–3072.
- [31] X.M. Han, H.K. Lee, Y.H. Lee, W. Hao, Y.J. Liu, I.Y. Phang, S.Z. Li, X.Y. Ling, Identifying enclosed chemical reaction and dynamics at the molecular level using shell-isolated miniaturized plasmonic liquid marble, J. Phys. Chem. Lett. 7 (2016) 1501–1506.
- [32] E.M.S. Lantman, T. Deckert-Gaudig, A.J.G. Mank, V. Deckert, B.M. Weckhuysen, Catalytic processes monitored at the nanoscale with tip-enhanced Raman spectroscopy, Nat. Nano. 7 (2012) 583–586.
- [33] M. Sun, Z. Zhang, Z.H. Kim, H. Zheng, H. Xu, Plasmonic scissors for molecular design, Chem. Eur. J. 19 (2013) 14958–14962.
- [34] Z.L. Zhang, S.X. Sheng, H.R. Zheng, H.X. Xu, M.T. Sun, Molecular resonant dissociation of surface-adsorbed molecules by plasmonic nanoscissors, Nanoscale 6 (2014) 4903–4908.
- [35] S. Chaunchaiyakul, A. Setiadi, P. Krukowski, F.C.I. Catalan, M. Akai-Kasaya, A. Saito, N. Hayazawa, Y. Kim, H. Osuga, Y. Kuwahara, Nanoscale dehydrogenation observed by tip-enhanced Raman spectroscopy, J. Phys. Chem. C 121 (2017) 18162–18168.
- [36] S. Linic, P. Christopher, D.B. Ingram, Plasmonic-metal nanostructures for efficient conversion of solar to chemical energy, Nat. Mater. 10 (2011) 911–921.
- [37] M.J. Kale, T. Avanesian, P. Christopher, Direct photocatalysis by plasmonic nanostructures, ACS Catal. 4 (2014) 116-128.
- [38] S. Linic, U. Aslam, C. Boerigter, M. Morabito, Photochemical transformations on plasmonic metal nanoparticles, Nat. Mater. 14 (2015) 567–576.
- [39] M.L. Brongersma, N.J. Halas, P. Nordlander, Plasmon-induced hot carrier science and technology, Nat. Nano. 10 (2015) 25–34.
- [40] R.T. Kidd, S.R. Meech, D. Lennon, Enhanced photodesorption of NO on roughened silver surfaces, Chem. Phys. Lett. 262 (1996) 142–150.
- [41] R.T. Kidd, D. Lennon, S.R. Meech, Surface plasmon enhanced substrate mediated photochemistry on roughened silver, J. Chem. Phys. 113 (2000) 8276–8282.
- [42] X. Chen, H.Y. Zhu, J.C. Zhao, Z.T. Zheng, X.P. Gao, Visible-light-driven oxidation of organic contaminants in air with gold nanoparticle catalysts on oxide supports, Angew. Chem. Int. Ed. 47 (2008) 5353–5356.
- [43] H. Zhu, X. Chen, Z. Zheng, X. Ke, E. Jaatinen, J. Zhao, C. Guo, T. Xie, D. Wang, Mechanism of supported gold nanoparticles as photocatalysts under ultraviolet and visible light irradiation, Chem. Comm. 7524–7526 (2009).
- [44] P. Christopher, H. Xin, S. Linic, Visible-light-enhanced catalytic oxidation reactions on plasmonic silver nanostructures, Nat. Chem. 3 (2011) 467–472.
- [45] K.H. Kim, K. Watanabe, D. Mulugeta, H.-J. Freund, D. Menzel, Enhanced photoinduced desorption from metal nanoparticles by photoexcitation of confined hot electrons using femtosecond laser pulses, Phys. Rev. Lett. 107 (2011).
- [46] P. Christopher, H. Xin, A. Marimuthu, S. Linic, Singular characteristics and unique chemical bond activation mechanisms of photocatalytic reactions on plasmonic nanostructures, Nat. Mater. 11 (2012) 1044–1050.

- [47] S. Mukherjee, F. Libisch, N. Large, O. Neumann, L.V. Brown, J. Cheng, J.B. Lassiter, E.A. Carter, P. Nordlander, N.J. Halas, Hot electrons do the impossible: plasmon-induced dissociation of H<sub>2</sub> on Au, Nano Lett. 13 (2013) 240–247.
- [48] T.-L.E. Wee, L.C. Schmidt, J.C. Scaiano, Photooxidation of 9-anthraldehyde catalyzed by gold nanoparticles: solution and single nanoparticle studies using fluorescence lifetime imaging, J. Phys. Chem. C 116 (2012) 24373–24379.
- [49] K.-H. Chen, Y.-C. Pu, K.-D. Chang, Y.-F. Liang, C.-M. Liu, J.-W. Yeh, H.-C. Shih, Y.-J. Hsu, Ag-nanoparticle-decorated SiO<sub>2</sub> nanospheres exhibiting remarkable plasmon-mediated photocatalytic properties, J. Phys. Chem. C 116 (2012) 19039–19045.
- [50] A. Marimuthu, J.W. Zhang, S. Linic, Tuning selectivity in propylene epoxidation by plasmon mediated photo-switching of Cu oxidation state, Science 339 (2013) 1590–1593
- [51] F. Wang, C.H. Li, H.J. Chen, R.B. Jiang, L.D. Sun, Q. Li, J.F. Wang, J.C. Yu, C.H. Yan, Plasmonic harvesting of light energy for Suzuki coupling reactions, J. Am. Chem. Soc. 135 (2013) 5588–5601.
- [52] S. Mukherjee, L. Zhou, A.M. Goodman, N. Large, C. Ayala-Orozco, Y. Zhang, P. Nordlander, N.J. Halas, Hot-electron-induced dissociation of H<sub>2</sub> on gold nanoparticles supported on SiO<sub>2</sub>, J. Am. Chem. Soc. 136 (2014) 64–67.
- [53] C. Boerigter, R. Campana, M. Morabito, S. Linic, Evidence and implications of direct charge excitation as the dominant mechanism in plasmon-mediated photocatalysis, Nat. Comm. 7 (2016) 10545.
- [54] C. Boerigter, U. Aslam, S. Linic, Mechanism of charge transfer from plasmonic nanostructures to chemically attached materials, ACS Nano 10 (2016) 6108-6115.
- [55] L. Yan, F. Wang, S. Meng, Quantum mode selectivity of plasmon-induced water splitting on gold nanoparticles, ACS Nano 10 (2016) 5452-5458.
- [56] D. Kumar, A. Lee, T. Lee, M. Lim, D.K. Lim, Ultrafast and efficient transport of hot plasmonic electrons by graphene for Pt free, highly efficient visible-light responsive photocatalyst, Nano Lett. 16 (2016) 1760–1767.
- [57] L. Zhou, C. Zhang, M.J. McClain, A. Manavacas, C.M. Krauter, S. Tian, F. Berg, H.O. Everitt, E.A. Carter, P. Nordlander, N.J. Halas, Aluminum nanocrystals as a plasmonic photocatalyst for hydrogen dissociation, Nano Lett. 16 (2016) 1478–1484.
- [58] H. Petek, Photoexcitation of adsorbates on metal surfaces: one-step or three-step, J. Chem. Phys. 137 (2012) 091704.
- [59] S. Tan, A. Argondizzo, J. Ren, L. Liu, J. Zhao, H. Petek, Plasmonic coupling at a metal/semiconductor interface, Nat. Photon. 11 (2017) 806-812.
- [60] S. Tan, Y. Dai, S. Zhang, L. Liu, J. Zhao, H. Petek, Coherent electron transfer at the Ag/graphite heterojunction interface, Phys. Rev. Lett. 120 (2018) 126801.
- [61] E. Kazuma, J. Jung, H. Ueba, M. Trenary, Y. Kim, Molecular photodissociation with visible light on metal surfaces, J. Am. Chem. Soc. 139 (2017) 3115–3121. [62] E. Kazuma, J. Jung, H. Ueba, M. Trenary, Y. Kim, Real-space and real-time observation of a plasmon-induced chemical reaction, Science 360 (2018) 521–526.
- [63] Y. Kim, K. Motobayashi, T. Frederiksen, H. Ueba, M. Kawai, Action spectroscopy for single-molecule reactions experiments and theory, Prog. Surf. Sci. 90 (2015) 85–143
- [64] X.H. Qiu, G.V. Nazin, W. Ho, Vibrationally resolved fluorescence excited with submolecular precision, Science 299 (2003) 542-546.
- [65] Y. Zhang, Y. Luo, Y. Zhang, Y.-J. Yu, Y.-M. Kuang, L. Zhang, Q.-S. Meng, Y. Luo, J.-L. Yang, Z.-C. Dong, J.G. Hou, Visualizing coherent intermolecular dipole-dipole coupling in real space, Nature 531 (2016) 623–627.
- [66] H. Imada, K. Miwa, M. Imai-Imada, S. Kawahara, K. Kimura, Y. Kim, Real-space investigation of energy transfer in heterogeneous molecular dimers, Nature 538 (2016) 364–367.
- [67] R. Zhang, Y. Zhang, Z.C. Dong, S. Jiang, C. Zhang, L.G. Chen, L. Zhang, Y. Liao, J. Aizpurua, Y. Luo, J.L. Yang, J.G. Hou, Nature 498 (2013) 82-86.
- [68] S.W. Wu, N. Ogawa, W. Ho, Atomic-scale coupling of photons to single-molecule junctions, Science 312 (2006) 1362-1365.
- [69] L. Bartels, F. Wang, D. Möller, E. Knoesel, T.F. Heinz, Real-space observation of molecular motion induced by femtosecond laser pulses, Science 305 (2004) 648–651.
- [70] M. Mehlhorn, H. Gawronski, K. Morgenstern, Diffusion and dimer formation of CO molecules induced by femtosecond laser pulses, Phys. Rev. Lett. 104 (2010) 076101.
- [71] H. Böckmann, S. Liu, J. Mielke, S. Gawinkowski, J. Waluk, L. Grill, M. Wolf, T. Kumagai, Direct observation of photoinduced tautomerization in single molecules at a metal surface, Nano Lett. 16 (2016) 1034–1041.
- [72] M.J. Comstock, N. Levy, A. Kirakosian, J. Cho, F. Lauterwasser, J.H. Harvey, D.A. Strubbe, J.M.J. Fréchet, S.G. Dirk Trauner, M.F. Crommie Louie, Reversible photomechanical switching of individual engineered molecules at a metallic surface, Phys. Rev. Lett. 99 (2007) 038301.
- [73] M. Bazarnik, L. Jurczyszyn, R. Czajka, K. Morgenstern, Mechanism of a molecular photo-switch adsorbed on Si(100), Phys. Chem. Chem. Phys. 17 (2015) 5366.
- [74] S. Grimme, J. Antony, S. Ehrlich, H. Krieg, A consistent and accurate ab initio parametrization of density functional dispersion correction (DFT-D) for the 94 elements H-Pu, J. Chem. Phys. 132 (2010) 154104.
- [75] S. Grimme, S. Ehrlich, L. Goerigk, Effect of the damping function in dispersion corrected density functional theory, J. Comp. Chem. 32 (2011) 1456-1465.
- [76] G. Kresse, D. Joubert, From ultrasoft pseudopotentials to the projector augmented-wave method, Phys. Rev. B 59 (1999) 1758-1775.
- [77] G. Kresse, J. Hafner, Ab initio molecular dynamics for liquid metals, Phys. Rev. B 47 (1993) 558-561.
- [78] G. Kresse, J. Furthmüller, Efficient iterative schemes for ab initio total-energy calculations using a plane-wave basis set, Phys. Rev. B 54 (1996) 11169–11186.
- [79] X.-Y. Zhu, Electronic structure and electron dynamics at molecule-metal interfaces: implications for molecule-based electronics, Surf. Sci. Rep. 56 (2004) 1–83.
- [80] G. Dutton, D.P. Quinn, C.D. Lindstrom, X.-Y. Zhu, Exciton dynamics at molecule-metal interfaces: C<sub>60</sub>/Au(111), Phys. Rev. B 72 (2005) 045441.
- [81] C.D. Lindstrom, D. Quinn, X.-Y. Zhu, Using image resonances to probe molecular conduction at the n-heptane/Au(111) interface, J. Chem. Phys. 122 (2005) 124714.
- [82] M. Bauer, S. Pawlik, M. Aeschlimann, Decay dynamics of photoexcited alkali chemisorbates: real-time investigations in the femtosecond regime, Phys. Rev. B 60 (1999) 5016–5028.
- [83] A.G. Borisov, J.P. Guayacq, E.V. Chulkov, V.M. Silkin, P.M. Echenique, Lifetime of excited electronic states at surfaces: comparison between the alkali/Cu(111) systems, Phys. Rev. B 65 (2002) 235434.
- [84] D.B. Boyd, Conformational dependence of the electronic energy levels in disulfides, J. Am. Chem. Soc. 94 (1972) 8799-8804.
- [85] Y.R. Lee, C.L. Chiu, S.M. Lin, Ultraviolet photodissociation study of CH<sub>3</sub>SCH<sub>3</sub> and CH<sub>3</sub>SSCH<sub>3</sub>, J. Chem. Phys. 100 (1994) 7376-7384.
- [86] A. Rinker, C.D. Halleman, M.R. Wedlock, Photodissociation dynamics of dimethyl disulfide, Chem. Phys. Lett. 414 (2005) 505-508.
- [87] C. Luo, W. Du, X. Duan, J. Liu, Z. Li, Theoretical study on the excited states and photodissociation mechanism of dimethyldisulfide, Chem. Phys. Lett. 469 (2009) 242–246.
- [88] L. Jensen, C.M. Aikens, G.C. Schatz, Electronic structure methods for studying surface-enhanced Raman scattering, Chem. Soc. Rev. 37 (2008) 1061-1073.
- [89] D.-Y. Wu, X.-M. Liu, S. Duan, X. Xu, B. Ren, S.-H. Lin, Z.-Q. Tian, Chemical enhancement effects in SERS spectra: a quantum chemical study of pyridine interacting with copper, silver, gold and platinum metals, J. Phys. Chem. C 112 (2008) 4195–4204.
- [90] A.M. Brown, R. Sundararaman, P. Narang, W.A. Goddard III, H.A. Atwater, Nonradiative plasmon decay and hot carrier dynamics: effects of phonons, surfaces, and geometry, ACS Nano 10 (2016) 957–966.
- [91] M. Ohara, Y. Kim, S. Yanagisawa, Y. Morikawa, M. Kawai, Role of molecular orbitals near the Fermi level in the excitation of vibrational modes of a single molecule at a scanning tunneling microscope junction, Phys. Rev. Lett. 100 (2008) 136104.
- [92] K. Motobayashi, Y. Kim, M. Ohara, H. Ueba, M. Kawai, The role of thermal excitation in the tunneling-electron-induced reaction: dissociation of dimethyl disulfide on Cu(111), Surf. Sci. 643 (2016) 18–22.
- [93] P. Maksymovych, D.B. Dougherty, X.-Y. Zhu, J.T. Yates Jr., Nonlocal dissociative chemistry of adsorbed molecules induced by localized electron injection into metal surfaces, Phys. Rev. Lett. 99 (2007) 016101.